HNUE JOURNAL OF SCIENCE
Natural Sciences 2024, Volume 69, Issue 3, pp. 87-95
This paper is available online at http://hnuejs.edu.vn/ns
DOI: 10.18173/2354-1059.2024-0038

STUDY ON GEOMETRICAL STRUCTURES AND ABSORPTION SPECTRA OF M_4^{2+} CLUSTERS (M = Cu, Ag, Au) ENCAPSULATED IN SAPO-42 ZEOLITE β-CAGE USING DENSITY FUNCTIONAL THEORY

Nguyen Thi Thuy Duong[1,2] and Ngo Tuan Cuong[1,2*]
[1]*Faculty of Chemistry, Hanoi National University of Education, Hanoi city, Vietnam*
[2]*Center for Computational Science, Hanoi National University of Education, Hanoi city, Vietnam*
[*]Corresponding author: Ngo Tuan Cuong, e-mail: cuongnt@hnue.edu.vn

Received August 14, 2024. Revised October 24, 2024. Accepted October 31, 2024.

Abstract. The most stable structures of tetrahedral M_4^{2+} cluster (M = Cu, Ag, Au) encapsulated in SAPO-42 zeolite β-cage have been determined by the DFT method using a/the B3LYP functional and LANL2DZ basis set. Electronic energies, zero point correction to energies and geometries, as well as the charge of the clusters, have been derived accordingly. The results showed that while the Cu-Cu bond length increases much when Cu_4^{2+} is in the framework, the Ag-Ag and Au-Au distances do not. The UV-Vis spectra of the $[M_4@SAPO\text{-}42]^{2+}$ clusters, which were calculated at the same hybrid B3LYP functional and the LANL2DZ basis set, show strong absorption peaks at 259 nm, 270 nm, and 259 nm for M being Cu, Ag, and Au, respectively. The nature of electronic transitions that are responsible for the absorption peaks in the UV-Vis spectrum of the $[M_4\text{-}SAPO\text{-}42]^{2+}$ clusters has been revealed.

Keywords: SAPO-42 zeolite, density functional theory (DFT), time-dependent density functional theory (TD-DFT), M_4^{2+} cluster.

1. Introduction

Coinage metal clusters have attracted significant interest for decades due to their fascinating properties and appealing structural beauty. The use of coinage metals in catalysis is one of their major industrial uses. Catalysts made of copper, silver, and gold have been used extensively [1]-[6].

Zeolites have a wide range of uses in our modern lifestyle, such as gas adsorption, water treatment, agriculture, animal feed additives, green chemistry, and petroleum refining, among many other uses. The most commonly used zeolite types are ZSM-5, Faujasite X, Y, and LTA. In terms of specific volume, zeolite LTA is one of the most

commonly used zeolites, while SAPO-42 is isostructural with zeolite LTA but shows a much lower cation-exchange capacity. The structures of SAPO molecular sieves include novel structure types as well as structure types analogous to certain zeolites [7]-[12].

Much research on the determination of structural characteristics and properties of SAPO-42 zeolite doping coinage metals has been done recently [13]-[16]. For example, the structure, location, and coordination of dehydrated Ag-SAPO-42 have been investigated by electron spin resonance and electron spin echo modulation spectroscopies [14]. Electron paramagnetic resonance (EPR) spectroscopy and Rietveld refinement are performed to identify the locations of active Cu^{2+} ions in Cu-SAPO-42 [15]. However, to our little knowledge of physicochemical and structural characterization, the detailed geometries of the coinage metal clusters doped into SAPO-42 zeolite or other zeolites are challenging due to the sensitivity to their sizes and geometries introduced by different experimental probes, which may lead to the formation of larger aggregates when examined with high-energy electron beams, X-ray irradiation. The effect of the tetrahedral M_4^{2+} cluster (M = Cu, Ag, Au) dopant on the change of geometries and properties of SAPO-42 zeolite has not been revealed and clarified yet.

With this up-to-date review, this work aims to study the optical properties of the tetrahedral M_4^{2+} cluster (M = Cu, Ag, Au) incorporated into SAPO-42 zeoliteβ-cage, namely geometrical and electronic structure, absorption UV-Vis spectra.

2. Content

2.1. Methods of calculation

In order to study the tetrahedral M_4^{2+} cluster (M = Cu, Ag, Au) encapsulated in SAPO-42 zeolite the method of density functional theory (DFT) and time-dependent density functional theory (TD-DFT) was used which are implemented in the Gaussian 09 software [17], [18].

Firstly, geometries of the tetrahedral M_4^{2+} clusters (M = Cu, Ag, Au) encapsulated in a SAPO-42 zeolite β-cage were optimized using the B3LYP/LANL2DZ functional and basis set [19]-[21]. These calculations were followed by frequency calculations to confirm that the stationary structures were minimal. Structural characteristics, relative energies, the electron configuration, and the charge of the clusters have also been investigated at the same level of theory.

Secondly, the TD-DFT calculation was performed at the optimized geometry to determine the energy levels of excited states and absorption spectra of the clusters.

2.2. Results and discussion

2.2.1. Geometries of the tetrahedral M_4^{2+} clusters (M = Cu, Ag, Au) in SAPO-42 zeolite β-cage

Stable isomers of the investigated clusters have been determined as follows. Firstly the Gaussview program has been used to construct all possible structures of M_4^{2+} clusters, namely the Y-shape, the rhombic, and the tetrahedral structures. These structures were

used for optimization calculations followed by frequency calculations. Stable isomers did not possess imaginary frequencies.

Then M_4^{2+} clusters were added into the stable structures of the modeled SAPO-42 zeolite β-cage forming the modeled $[M_4\text{-SAPO-42}]^{2+}$ clusters which are the input structures for the next optimization calculations. The most stable optimized structures of the clusters have been illustrated in Figure 1.

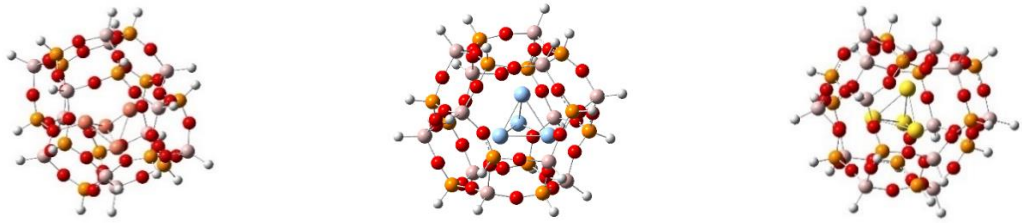

a) $[Cu_4\text{-SAPO-42}]^{2+}$ cluster b) $[Ag_4\text{-SAPO-42}]^{2+}$ cluster c) $[Au_4\text{-SAPO-42}]^{2+}$ cluster

Figure 1. Geometries of the most stable isomers of $[M_4\text{-SAPO-42}]^{2+}$ (M = Cu, Ag and Au) cluster which are optimized at B3LYP/LANL2DZ level of theory

The most stable isomer of the M_4^{2+} cluster has a tetrahedral structure and belongs to the T_d point group. When loading the tetrahedral M_4^{2+} cluster (M = Cu, Ag, Au) into the SAPO-42 zeolite β-cage, the symmetry of M_4 clusters is all reduced, and the framework is also deformed.

$[Cu_4\text{-SAPO-42}]^{2+}$. The length of the Cu-Cu bond in the Cu_4^{2+} cluster is 2.54 Å. When loaded into SAPO-42 zeolite, the Cu-Cu average bond length is 2.59 Å slightly larger than the Cu-Cu bond length in the Cu_4^{2+} cluster. This indicates that the Cu_4^{2+} cluster interacts with the SAPO-42 zeolite β-cage to a significant extent.

$[Ag_4\text{-SAPO-42}]^{2+}$. The length of the Ag-Ag bond in the Ag_4^{2+} cluster is 2.90 Å. When loaded into SAPO-42 zeolite, the Ag-Ag average bond length is 2.87 Å slightly smaller than the Ag-Ag bond length in the Ag_4^{2+} cluster, and this shows that the interaction of the Ag_4^{2+} cluster and the framework is rather weak. The symmetry of the Ag_4^{2+} cluster is reduced from the T_d to the C_{3v} point group.

$[Au_4\text{-SAPO-42}]^{2+}$. The length of the Au-Au bond in the Au_4^{2+} cluster is 2.82 Å. When loaded into SAPO-42 zeolite, the Au-Au average bond length is 2.79 Å slightly smaller than the Au-Au bond length in the Au_4^{2+} cluster.

2.2.2. Properties of the $[M_4\text{-SAPO-42}]^{2+}$ clusters

Electronic energies and zero-point energies of the $[M_4\text{-SAPO-42}]^{2+}$ clusters

Table 1. Electronic energies and zero-point energies of the $[M_4\text{-SAPO-42}]^{2+}$ clusters (M = Cu, Ag and Au)

Cluster	Electronic energies (HF, a.u)	Zero-point energies (ZPE, a.u)	The sum of electronic and zero-point energies E=HF + ZPE (a.u)
$[Cu_4\text{-SAPO-42}]^{2+}$	-3610.6643121	0.390655	-3610.27366
$[Ag_4\text{-SAPO-42}]^{2+}$	-3409.1439067	0. 3878448	-3408.756062
$[Au_4\text{-SAPO-42}]^{2+}$	-3367.8497553	0.3886409	-3367.461114

Charges of the $[M_4\text{-SAPO-42}]^{2+}$ clusters

In the M_4^{2+} free cluster, the +2 charge equally spread on each M atom, making the charge on each M atom being +0.5.

From the most stable isomers of $[M_4\text{-SAPO-42}]^{2+}$ clusters, NBO charges on M_4 clusters and the SAPO-42 zeolite framework were computed. The results are listed in Table 2.

Table 2. Charge of the M_4 cluster and SAPO-42 framework in the $[M_4\text{-SAPO-42}]^{2+}$ clusters (M = Cu, Ag and Au)

Cluster	NBO charge of the M_4 cluster and SAPO-42 zeolite	
	M_4	***SAPO-42 framework***
$[Cu_4\text{-SAPO-42}]^{2+}$	+1.135	+0.865
$[Ag_4\text{-SAPO-42}]^{2+}$	+1.109	+0.891
$[Au_4\text{-SAPO-42}]^{2+}$	+0.935	+1.065

It was discovered that the +2 charge on the whole modeled cluster $[M_4\text{-SAPO-42}]^{2+}$ is well distributed between the M_4 cluster and the SAPO-42 β-cage, making a ca.+1 charge on each part of the modeled cluster.

2.2.2. UV-Vis absorption spectra of the $[M_4\text{-SAPO-42}]^{2+}$ clusters

Using the TD-DFT method implemented in the Gaussian 09 package, the absorption spectra of the clusters were simulated. From there, the absorption spectrum of the ultraviolet-visible region of the studied clusters and the origin of their spectral peaks were plotted.

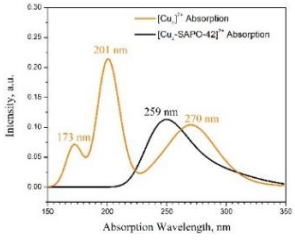

a) $[Cu_4\text{-SAPO-42}]^{2+}$ cluster

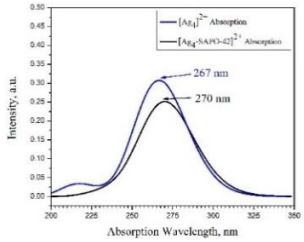

b) $[Ag_4\text{-SAPO-42}]^{2+}$ cluster

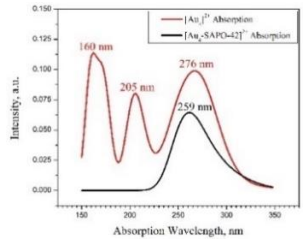

c) $[Au_4\text{-SAPO-42}]^{2+}$ cluster

Figure 2. UV-Vis spectral images of the M_4^{2+} bare cluster and the $[M_4\text{-SAPO-42}]^{2+}$ modelled cluster (M = Cu, Ag and Au)

TD-DFT calculations are performed at the optimized geometry of $[Cu_4\text{-SAPO-42}]^{2+}$ modelled cluster using B3LYP/LANL2DZ method and several lower-lying singlet excited states can thereby be identified. The corresponding optical absorption spectrum is shown in Figure 2, and the electron transitions are summarized in Table 3. The absorption spectrum of the $[Cu_4]^{2+}$ bare cluster has three peaks, and the one with the lowest excitation energy at 270 nm due to the HOMO – 3 ⟶ LUMO, LUMO+1 and LUMO+2 transitions. The other peaks are centered at 173 nm and 201 nm. When being inside the SAPO-42 zeolite β-cage, the absorption wavelength at 270 nm shifts to the higher energy region, at 259 nm. This absorption band dues to the HOMO-8, HOMO – 1 ⟶ LUMO + 2 electronic transitions. This band has the same feature as the band at 270 nm in the absorption spectrum of the Cu_4^{2+} bare cluster, being the electron transition from the *s* and *d* orbitals to the *s* orbitals of Cu atoms, with some contribution from orbitals of O atoms in the framework.

Table 3. Nature of electronic transitions that responsible for the absorption peaks in the UV-Vis spectrum of the $[Cu_4]^{2+}$ cluster and the $[Cu_4$-SAPO-42$]^{2+}$ cluster

Cluster	Band	Transitions	ΔE (eV)	λ (nm)	f	MO Contribution	Theoretical Assignment
$[Cu_4]^{2+}$	A	I	4.60	270	0.0780	H-3 ⟶ L 20% H-3 ⟶ L+1 9%	s, d (Cu) ⟶ s (Cu)
		II	4.60	270	0.0780	H-3 ⟶ L 9% H-3 ⟶ L+1 20%	
		III	4.60	270	0.0780	H-3 ⟶ L+2 29%	
	B	IV	6.18	201	0.2143	H-20 ⟶ L 28% H-20 ⟶ L+1 43%	s, d (Cu) ⟶ s (Cu)
		V	6.18	201	0.2143	H-20 ⟶ L 43% H-20 ⟶ L+1 28%	
		VI	6.18	201	0.2143	H-20 ⟶ L+2 71%	
	C	VII	7.26	173	0.0600	H-2 ⟶ L+5 28% H ⟶ L+6 28%	d (Cu) ⟶ s, p (Cu)
		VIII	7.26	173	0.0600	H-1 ⟶ L+5 28% H ⟶ L+4 28%	
		IX	7.26	173	0.0600	H-2 ⟶ L+4 30% H-1 ⟶ L+6 30%	
$[Cu_4$-SAPO-42$]^{2+}$	A	I	4.78	259	0.0477	H-8 ⟶ L+2 18% H-1 ⟶ L+2 22%	s, d (Cu) ⟶ s (Cu), and O framework

The absorption spectrum of the $[Ag_4]^{2+}$ bare cluster has only one peak with a maximum absorption wavelength at 267 nm due to the HOMO ⟶ LUMO, LUMO+1 and LUMO+2 transitions. When loaded into the SAPO-42 zeolite β-cage, the maximum absorption wavelength of the cluster does not shift significantly, being at 270 nm. This absorption band also dues to the HOMO ⟶ LUMO, LUMO+1, and LUMO+2 transitions, being the electron transitions from the *s* orbitals to the *s* and *p* orbital of Ag atoms, with the contribution of orbitals of O atoms in the SAPO-42 β-cage.

Table 4. Nature of electronic transitions that responsible for the absorption peaks in the UV-Vis spectrum of the $[Ag_4]^{2+}$ bare cluster and the $[Ag_4$-SAPO-42$]^{2+}$ cluster

Cluster	Band	Transition	Δ*E* (eV)	λ (nm)	f	MO Contribution	Theoretical Assignment
$[Ag_4]^{2+}$	A	I	4.65	267	0.3076	H ⟶ L 90%	s (Ag) ⟶ s, p (Ag)
		II	4.65	267	0.3076	H ⟶ L+2 90% H ⟶ L+1 14%	
		III	4.65	267	0.3076	H ⟶ L+1 90% H ⟶ L+2 14%	
$[Ag_4$-SAPO-42$]^{2+}$	A	I	4.54	273	0.2455	H ⟶ L 94%	s (Ag), O framework ⟶ s, p (Ag), O framework
		II	4.59	270	0.2482	H ⟶ L+1 92%	
		III	4.60	269	0.2477	H ⟶ L+2 92%	

The absorption spectrum of the $[Au_4]^{2+}$ bare cluster has three peaks, and the longest wavelength one 276 nm due to the HOMO– 11 ⟶ LUMO, LUMO + 1 and LUMO + 2 transitions. The other peaks are at 205 nm and 160 nm. When Au_4^{2+} is in the SAPO-42 zeolite β-cage, the maximum absorption wavelength shifts to the shorter one, at 259 nm. This absorption band dues to the HOMO - 15, HOMO – 14 ⟶ LUMO transitions.

Table 5. Nature of electronic transitions that are responsible for the absorption peaks in the UV-Vis spectrum of the $[Au_4]^{2+}$ cluster and the $[Au_4$-SAPO-42$]^{2+}$ cluster

Cluster	Band	Transition	Δ*E* (eV)	λ (nm)	f	MO Contribution	Theoretical Assignment
$[Au_4]^{2+}$	A	I	4.49	276	0.0881	H-11 ⟶ L+1 68%	s, d (Au) ⟶ s (Au)
		II	4.49	276	0.0881	H-11 ⟶ L 68%	

		III	4.49	276	0.0881	H-11 ⟶ L+2 70%	
	B	IV	6.06	205	0.0942	H-18 ⟶ L+2 38% H-17 ⟶ L+1 38%	d (Au) ⟶ s, p (Au)
		V	6.06	205	0.0942	H-19 ⟶ L+2 38% H-17 ⟶ L 38%	
		VI	6.06	205	0.0942	H-19 ⟶ L+1 39% H-18 ⟶ L 39%	
	C	VII	7.75	160	0.1138	H-2 ⟶ L+5 37% H-1 ⟶ L+6 37%	d (Au) ⟶ s, p (Au)
		VIII	7.75	160	0.1138	H-2 ⟶ L+4 37% H ⟶ L+6 37%	
		IX	7.75	160	0.1137	H-1 ⟶ L+4 42% H ⟶ L+5 42%	
$[Au_4$-SAPO-42$]^{2+}$	A	I	4.78	259	0.0328	H-15 ⟶ L 49% H-14 ⟶ L 15%	d (Au), O framework ⟶ s (Au)

3. Conclusions

A new B3LYP functional and LANL2DZ basis set has been employed to optimize geometrical structures following by frequency calculations of the tetrahedral M_4^{2+} cluster (M = Cu, Ag, Au) encapsulated in SAPO-42 zeolite forming $[M_4$-SAPO-42$]^{2+}$ clusters. Electronic energies, zero point energies, and geometries of the clusters have been derived.

The changes in geometry, and average M-M (M = Cu, Ag, Au) bond lengths of the $[M_4$-SAPO-42$]^{2+}$ clusters have also been determined.

The UV-Vis spectra of the $[M_4\text{-SAPO-42}]^{2+}$ clusters have been investigated using the TD-DFT method with the hybrid B3LYP functional and the LANL2DZ basis set. The prediction absorption spectra of the $[M_4\text{-SAPO-42}]^{2+}$ clusters were characterized by strong absorption peaks at 259 nm, 270 nm, and 259 nm for the $[Cu_4\text{-SAPO-42}]^{2+}$ cluster, $[Ag_4\text{-SAPO-42}]^{2+}$ cluster and $[Au_4\text{-SAPO-42}]^{2+}$ cluster, respectively. The electronic transitions that responsible for the absorption peaks in the UV-Vis spectrum of the $[M_4\text{-SAPO-42}]^{2+}$ cluster are from *s*-, *d*-AOs of Cu to *s*-AOs of Cu and *s*-, *p*-AOs of O in the framework, from *s*-AOs of Ag to the *s*-, *p*- of Ag combined with *s*-, *p*-AOs of O framework, as well as from *d*-AOs of Au and *s*-, *p*-AOs of O framework to the *s*-AOs of Au.

Acknowledgements. The authors would like to thank the Center for Computational Science, Hanoi National University of Education for the computational facilities.

REFERENCES

[1] Lu Y, Wei W & Chen W, (2012). Copper nanoclusters: Synthesis, characterization and properties. *Chinese Science Bulletin*, 57(1), 41-47.

[2] Yin B & Luo Z, (2021). Coinage metal clusters: From superatom chemistry to genetic materials. *Coordination Chemistry Reviews*, 429, 213643. DOI:10.1016/j.ccr.2020.213643.

[3] Hongxin Si, Tong Shu, Xin Du, Lei Su & Xueji Zhang, (2022), An Overview on Coinage Metal Nanocluster-Based Luminescent Biosensors via Etching Chemistry. *Biosensors*, 12(7), 511.

[4] Nguyen TTH, Nguyen TMH, Bui CT, Nguyen NH & Le MC, (2019). Study on the Adsorption and Activation Behaviours of Carbon Dioxide over Copper Cluster (Cu_4) and Alumina-Supported Copper Catalyst (Cu_4/Al_2O_3) by means of Density Functional Theory. *Journal of Chemistry*, 1, 10. DOI:10.1155/2019/4341056.

[5] Edward IS, David EH, Esther MJ, Jake WG, Jordi C, Munzarin Q, Matthew TKE, Christian HK, Ryan G. Hadt & Li T, (2014). Copper Active Sites in Biology. *Chemical Reviews*, 114(7), 3659-3853. DOI:10.1021/cr400327t.

[6] Le TMO, Lam TH, Pham TN, Ngo TC, Lai ND, Do DB & Nguyen VM, (2018). Enhancement of Rhodamine B Degradation by Ag Nanoclusters-Loaded g-C3N4 Nanosheets. *Polymers*, 10, 633. https://www.mdpi.com/2073-4360/10/6/633.

[7] Collins F, Rozhkovskaya A, Outram JG & Millar GJ, (2019). A critical review of waste resources, synthesis, and applications for Zeolite LTA. *Microporous and Mesoporous Materials*, 290, 109668. DOI:10.1016/j.micromeso. 2019.1096.

[8] Martínez-Franco R, Cantín Á, Vidal-Moya A, Moliner M & Corma A, (2015). Self-Assembled Aromatic Molecules as Efficient Organic Structure Directing Agents to Synthesize the Silicoaluminophosphate SAPO-42 with Isolated Si Species. *Chemistry of Materials*, 27(8), 2981-2989. DOI:10.1021/acs.chemmater.5b00337.

[9] Kühl GH & Schmitt KD, (1990). Reexamination of phosphorus-containing zeolites ZK-21 and ZK-22 in light of SAPO-42 Zeolites, 10(1), 2-7. DOI:10.1016/0144-2449(90)90086-7.

[10] Pinilla-Herrero I, Olsbye U, Márquez-Álvarez C & Sastre E, (2017). Effect of framework topology of SAPO catalysts on selectivity and deactivation profile in the methanol-to-olefins reaction. *Journal of Catalysis*, 352, 191-207. DOI:10.1016/j.jcat.2017.05.008.

[11] Pinilla-Herrero I, Márquez-Álvarez C, Sastre E, 2017. The complex relationship between SAPO framework topology, content, distribution of Si, and catalytic behaviour in the MTO reaction. *Catalysis Science & Technology*, 7(17), 3892-3901. DOI:10.1039/c7cy01250k.

[12] Pérez-Botella E, Martínez-Franco R, González-Camuñas N, Cantín Á, Palomino M, Moliner M, Valencia S & Rey F, (2020). Unusually Low Heat of Adsorption of CO2 on AlPO and SAPO Molecular Sieves. *Frontiers in Chemistry*, 8, 588712. DOI: 10.3389/fchem.2020.588712.

[13] Pierloot K, Delabie A, Groothaert MH, Schoonheydt RA, (2001). A reinterpretation of the EPR spectra of Cu(II) in zeolites A, Y, and ZK4, based on ab initio cluster model calculations. *Physical Chemistry Chemical Physics*, 3(11), 2174-2183. DOI:10.1039/b100531f .

[14] Michalik J, Zamadics M, Sadlo J & Kevan L, (1993). Electron spin resonance and electron spin echo modulation studies on radiation-induced silver agglomeration in a SAPO-42 molecular sieve: a comparison with isostructural zeolite A. *The Journal of Physical Chemistry*, 97(40), 10440-10444. DOI:10.1021/j100142a029.

[15] Nana Y, Chao M, Yi C, Xiaona L, Lei C, Peng G, Peng T & Zhongmin L, (2020). Rational Design of a Novel Catalyst Cu-SAPO-42 for NH_3-SCR Reaction. *Small*, 16 (33), 2000902. DOI:10.1002/smll.202000902.

[16] Didier G, Eduardo CG, Ngo TC, Eduard F, Wouter B, Saleh A, Philomena S, Francesco DA, Dipanjan B, Maarten BJR, Nguyen MT, Johan H & Peter L, (2018). Origin of the bright photoluminescence of few-atom silver clusters confined in LTA zeolites. *Science*, 361(6403), 686-690.

[17] Frisch MJ, Schlegel HB, Scuseria GE, Robb MA, Cheeseman JR, Montgomery JA & et al., (2009). (Gaussian 09 Revision: D.01, 2009), Gaussian 09 Revision: D.01.

[18] Hohenberg P & Kohn W, 1964. Inhomogeneous Electron Gas. *Physical Review B*, 136, 864.

[19] Becke AD, (1993). Density-functional thermochemistry. III. The role of exact exchange. *Journal of Chemical Physics*, 98, 5648.

[20] Perdew JP, Burke K & Ernzerhof M, (1996). Generalized gradient approximation made simple. *Physical Review Letters*, 77, 3865.

[21] Hay PJ & Wadt WR, (1998). Ab initio effective core potentials for molecular calculations-potentials for the transition-metal atoms Sc to Hg. *Journal of Chemical Physics*, 82, 270.